HHS Public Access

Author manuscript

J Control Release. Author manuscript; available in PMC 2018 July 16.

Published in final edited form as:

J Control Release. 2017 June 28; 256: 1–8. doi:10.1016/j.jconrel.2017.04.017.

Enhancing tissue permeability with MRI guided preclinical focused ultrasound system in rabbit muscle: from normal tissue to VX2 tumor

Yao Sun[1,*], **Xiaobing Xiong**[1,*], **Darpan Pandya**[2], **Youngkyoo Jung**[1,3], **Akiva Mintz**[1,2], **Satoru Hayasaka**[4], **Thaddeus J. Wadas**[1,2,3], and **King C.P. Li**[5]

[1]Department of Radiology, Wake Forest School of Medicine, Winston-Salem, NC 27157, USA

[2]Comprehensive Cancer Center, Wake Forest School of Medicine, Winston-Salem, NC 27157, USA

[3]Department of Biomedical Engineering, Wake Forest School of Medicine, Winston-Salem, NC 27157, USA

[4]Department of Psychology, The University of Texas at Austin, SEA 2.214, 108 E. Dean Keeton Stop A8000, Austin, TX 78712, USA

[5]Carle Illinois College of Medicine, University of Illinois at Urbana- Champaign, Urbana, IL 61801, USA

Abstract

High Intensity Focused Ultrasound (HIFU) is an emerging noninvasive, nonionizing physical energy based modality to ablate solid tumors with high power, or increase local permeability in tissues/tumors in pulsed mode with relatively low power. Compared with traditional ablative HIFU, nondestructive pulsed HIFU (pHIFU) is present in the majority of novel applications recently developed for enhancing the delivery of drugs and genes. Previous studies have demonstrated the capability of pHIFU to change tissue local permeability for enhanced drug delivery in both mouse tumors and mouse muscle. Further study based on bulk tissues in large animals and clinical HIFU system revealed correlation between therapeutic effect and thermal parameters, which was absent in the previous mouse studies. In this study, we further investigated the relation between the therapeutic effect of pHIFU and thermal parameters in bulky normal muscle tissues based on a rabbit model and a preclinical HIFU system. Correlation between therapeutic effect and thermal parameters was confirmed in our study on the same bulk tissues although different HIFU systems were used. Following the study in bulky normal muscle tissues, we further created bulky tumor model with VX2 tumors implanted on both hind limbs of rabbits and investigated the feasibility to enhance tumor permeability in bulky VX2 tumors in a rabbit

Correspondence should be addressed to King C.P. Li (kingli@illinois.edu) or Akiva Mintz (amintz@wakehealth.edu).
*These authors contributed equally to this work.

Chemical compounds studied in this article: ^{111}In chloride ($InCl_3$) (PubChem CID: 24812)

model using pHIFU technique. A radiolabeled peptidomimetic integrin antagonist, ^{111}In-DOTA-IA, was used following pHIFU treatment in our study to target VX2 tumor and serve as the radiotracer for follow-up single-photon emission computed tomography (SPECT) scanning. The results have shown significantly elevated uptake of ^{111}In-DOTA-IA in the area of VX2 tumors pretreated by pHIFU compared with the control VX2 tumors not being pretreated by pHIFU, and statistical analysis revealed averaged 34.5% enhancement 24hours after systematic delivery of ^{111}In-DOTA-IA in VX2 tumors pretreated by pHIFU compared with the control VX2 tumors.

Graphical abstract

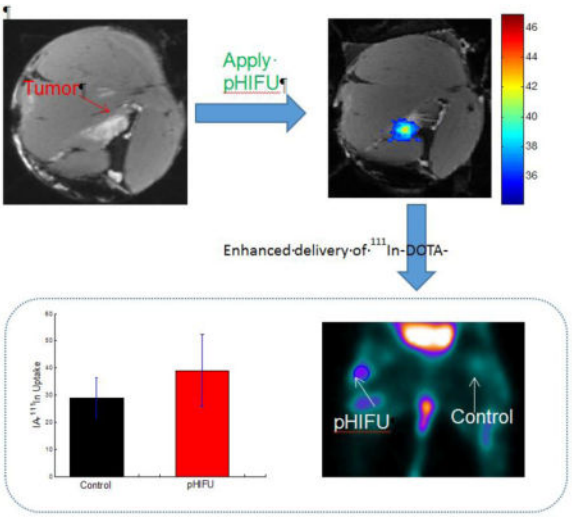

Keywords

Tissue permeability; VX2 tumor; Translational study; Rabbit model; High intensity focused ultrasound; Image guided drug delivery; ^{111}In; MRI; SPECT

1. Introduction

HIFU is an emerging therapeutic technique to noninvasively deliver localized ultrasound energy deep in the body without affecting the surrounding tissues.[1] Currently it has been in clinical use or under clinical trial as an alternate approach to open surgery to noninvasively ablate a variety of tumors, such as uterine fibroids, prostate tumor, brain tumor, breast tumor, etc.[2–8] Although tumor ablation with high power is the best known application of HIFU technology, there is increasing interest in using the same HIFU technology in pulsed mode with relatively low power – pulsed HIFU (pHIFU) – to nondestructively create change in tissue permeability for enhancing the delivery of therapeutic agents in the tumor. For example, studies have shown that pHIFU exposure can lead to improved delivery of high-molecular weight fluorophore, plasmid DNA, fluorescently labeled polystyrene nanoparticles, monoclonal antibodies, and tissue plasminogen activator (tPA).[9–14] Combined with microbubbles, HIFU exposure in brain has been used to locally disrupt the intact blood–brain barrier (BBB) to allow penetration of IgG tracer.[15]

Although the therapeutic benefits of pHIFU for drug delivery enhancement has been well-established in mouse models, there was little studies on the mechanism of pHIFU enhanced drug delivery. The correlation between treatment parameters and treatment effects is still elusive, which hinders the translational and clinical application of pHIFU technique to enhance localized drug delivery in tumors. For example, recent study based on bulk tissue in large animals and clinical HIFU system have revealed correlation between therapeutic effect and thermal parameters,[16] the findings of which differs significantly from the results reported in previous mouse studies.[17, 18] In this study, we further investigated the relation between the therapeutic effect of pHIFU and thermal parameters in bulky normal muscle tissues based on a rabbit model and a preclinical HIFU system, with the goal to validate the previous findings and investigate the translational feasibility of pHIFU drug delivery from mouse to clinical models. Following the mechanism study between the therapeutic effects of pHIFU and thermal parameters on bulky normal muscle tissues, we further investigated the feasibility of using pHIFU technique to enhance tumor permeability in bulky VX2 tumors implanted in rabbits. A radiolabeled peptidomimetic integrin antagonist ^{111}In-DOTA-IA was used following pHIFU treatment in our study to target VX2 tumor and serve as the radiotracer for the enhanced drug delivery study. The uptake of ^{111}In-DOTA-IA in the area of VX2 tumors pretreated by pHIFU was then compared by SPECT imaging with that in control VX2 tumors not being pretreated by HIFU.

2. Materials and Methods

2.1 Animal Experiments

Eleven female New Zealand white rabbits (Robinson Services Inc., Mocksville, NC) between 3 and 4 kg in weight were used in the study. Five of the rabbits were implanted with VX2 tumors, four of which successfully completed all the procedures in the study. Eight successful pHIFU experiments were conducted on the remaining six rabbits for the purpose of optimizing the pHIFU treatment parameters and investigating its correlation with the therapeutic effects of pHIFU treatment. All animals were handled according to a protocol approved by the Institutional Animal Care and Use Committee of Wake Forest School of Medicine. During pHIFU treatment, rabbits were sedated with intramuscular injection of 25mg/kg ketamine and 4mg/kg xylazine. The injection consists of 100 mg/ml of ketamine and 20 mg/ml of xylazine (mixture). The surgical anesthesia was maintained with 2%–3% isoflorane inhalation anesthesia. Prior to procedure, their hair was clipped over the hind limbs on the side to be treated and the remaining hair was removed using a medical depilatory. In the study of investigating the correlation between the therapeutic effects of pHIFU treatment and the thermal parameters, the muscle tissue on both hind limbs of rabbits will be treated by pHIFU with a 3–4 weeks recovery gap between the two experiments. Following terminal MRI or SPECT scanning, rabbits were euthanized by intravenous administration of Pentobarbital Sodium 120mg/kg.

2.2 VX2 tumor implantation

Intramuscular VX2 carcinomas were implanted in the gluteal muscles on both sides of five rabbits to be treated by HIFU. The VX2 carcinoma tumor cells were purchased from the NCI-DTP tumor repository. Rabbits were sedated with intramuscular injection of 25mg/kg

ketamine and 4mg/kg xylazine. The injection consists of 100 mg/ml of ketamine and 20 mg/ml of xylazine (mixture). Immediately before the procedure, lateral aspects of the hind limb of rabbits were locally shaved and disinfected using alcohol spray. 0.75–1.0 mL of VX2 cell solution (800,000 cells/kg rabbit weight) were then injected deep in the gluteal muscles of hind limbs of the rabbits. Around 7 days after inoculation the tumors were expected to reach an average size of about 500 mm^3. The tumors in one of the five rabbits implanted with VX2 tumors did not grow well and did not enter the pHIFU treatment study. The other four successfully completed all the procedures in the study.

2.3 HIFU treatment

The HIFU treatment was conducted with a customized MRI/MR thermometry-guided preclinical HIFU unit (RK-100, FUS Instruments Inc., Toronto, Ontario, Canada) to deliver ultrasound energy to the target sites in the hind limb of rabbits. The system probe is a spherically focused ultrasound transducer with a center frequency of 1MHz and a focal spot size around 1–2mm in diameter and 5–6mm in length. The focal length of the probe is 60mm. The probe is mounted on a MR-compatible computer-controlled three-axis positioner to allow for precisely focusing on the targeted site. The probe is immersed in a tank full of degassed and deionized water for acoustic coupling. Prior to the HIFU treatment, the focal spot is registered with the MR coordinates with a method established before[19]. The rabbit was rest prone lateral in the water tank on a gel pad with ultrasound transparent film on the bottom. During treatment, the focused spot was placed against the hind limb of the rabbit (the side to receive HIFU treatment). The surface of the probe was kept around 50–55mm below the rabbit skin to allow for precise focusing on the target spot in the target spot in the muscle tissue, which is typical 5–10mm beneath the rabbit skin. The distance from the probe surface and the skin of rabbit may vary a little bit, depending on the spot location in the muscle. The acoustic parameters during the pHIFU treatment are in the range of 60–90W peak acoustic power (P^{Peak}), 5–20% duty cycle (DC) and 120–240 pulses (1Hz) per sonication, which are based on reported studies[16, 20] and then further optimized experimentally on our customized preclinical pHIFU system to reach the targeted therapeutic effect. The maximum deliverable peak power of our system is around 90W, which is much lower than that in clinical pHIFU system (>280W) used in previous studies. As such, duty cycle and number of pulses were increased during our study in comparison to the acoustic parameters used in reported studies, in order to reach the threshold (average power > 10.25W) for successful pHIFU treatment found before.[16] The acoustic intensity around the focused spot and the HIFU induced temperature change in each experiment was controlled and monitored in near real-time by using MR-thermometry.

2.4 MRI and MR thermometry

The MRI scans were conducted with a customized surface coil (FUS Instruments Inc., Toronto, Ontario, Canada) attached to a 3T Siemens Skyra scanner (Siemens, Erlangen, Germany) to acquire all MRI images to guide the treatment, monitor the temperature profiles during the treatment, visualize the induced edema in T2-weighted images before and after treatment, and analyze the permeability changes with T1-weighted dynamic contrast enhanced (DCE) MRI images.

Image guidance was based on T2-weighted images acquired by MRI using 3D dual echo steady-state sequence (echo time (TE)/repetition time (TR)= 5.7/17ms, 10cm field of view (FOV), 256 × 256 matrix size, 88 slices, 0.39×0.39 mm2 in-plane resolution, 0.4mm slice thickness, and 5 min. scan time). The same MRI sequence was used to detect edema in normal tissue treated by HIFU. Edema was detected by comparing T2-weighted images from before and after treatment.

The temperature monitoring was performed based on MR thermometry using a 2D gradient echo sequence (baseline temperature: 37°C, TE/TR=8.7/30ms, 10cm FOV, 128 × 128 matrix, 5 slices, 6/8 partial Fourier factor, 0.78 × 0.78mm^2 in-plane resolution, 5 mm slice thickness, and 14.5 s temporal resolution). A reference phase image was acquired prior to HIFU treatment and the temperature was estimated by calculating the phase difference between the present phase during heating and the reference phase in the treatment area. Another area outside the treatment area was also chosen to correct the magnetic field drift during the HIFU treatment. The temperature maps covering the treatment area were updated and monitored in every time frame (14.5 sec).

T1-weighted contrast enhanced (CE) images were extracted from the DCEMRI series 7 min after bolus injection of 4 ml gadopentetate dimeglumine (Magnevist®; Bayer HealthCare Pharmaceuticals Inc., Wayne, NJ) over 20 second to verify the change of tissue permeability in the treated site immediately after (0 hours) and 24 hours after HIFU treatment. The concentration of gadopentetate dimeglumine used in our study is 0.5 mmole/ml. The DCEMRI series was acquired by T1 mapping images using flip angles of 10, 20, 30, 50 and 70, and dynamic contrast enhanced imaging, DCEMRI (TE = 2.62 ms, TR = 6.0ms, FOV 180 mm × 180 mm, acquisition matrix 192 × 192, pixel spacing 0.9375 mm × 0.9375 mm, NEX = 1, temporal resolution 10.44 s). The full DCEMRI curves were fit to the Kety model using Nelder-Mead simplex curve fitting and the permeability k^{trans} was produced quantitatively.

2.5 Post-processing of the MR thermometry data

Temperature maps were reconstructed using the PRF method and based on the assumption of a core temperature of 37°C. The thermal dose standard CEM_{43} was used to calculate the accumulative thermal dose during the HIFU treatment, which is based on the following standard definition:[21]

$$CEM_{43} = \int_0^{t_e} R^{[43 - T(t)]} dt, R = \begin{cases} 0.25, & T \le 43°C \\ 0.5, & T > 43°C \end{cases} \quad (1)$$

where CEM_{43} is the “thermal iso-effective dose” in “cumulative equivalent minutes” at 43°C, T(t) is temperature at time t, and t_e is the end time of the HIFU treatment. This equation was applied for each voxel to calculate the thermal dose map in the treated region.

2.6 ^{111}In-DOTA-IA synthesis

To demonstrate the enhanced permeability of the tumor treated by pHIFU, we used a small molecule $\alpha_v\beta_3$ targeting radiopharmaceutical ^{111}In-DOTA-IA, which has been shown in a previous study to maintain a high affinity towards $\alpha_V\beta_3$ positive tumor without the shortcoming of high non-specific renal uptake[22]. The radiopharmaceutical ^{111}In-DOTA-IA was synthesized by radiolabeling tumor targeting IA with ^{111}In using DOTA as a bifunctional chelator. The synthesis of ^{111}In-DOTA-IA has been previously reported.[22, 23] In brief, ^{111}In (2−3mCi, 74–111MBq) in 100μL of 1 M NH_4OAc buffer (pH 6.0) was added to 5μg of DOTA-IA in 100μL of 1 M NH_4OAc buffer (pH 6.0). The reaction mixture was incubated at 90°C for 30 min. The reaction was monitored by radio-TLC using Varian ITLC-SG strips developed with 50 mM EDTA (pH 5.5). In this system, free ^{111}In forms a complex with EDTA and eluted with the solvent front ($R_f = 1$), while ^{111}In-DOTA-IA remained at origin ($R_f = 0$). 4ml of the synthesized ^{111}In-DOTA-IA (2.37mCi) was intravenously injected into the rabbits one day after receiving pHIFU treatment.

2.7 SPECT Scanning

One day following intravenous injection, SPECT scanning was performed on a Philips Brightview XCT Dual-detector scanner with 64 projections using bone windows centered at 30 second stops and ^{111}In windows. 3-D images were then reconstructed. DICOM images were later analyzed with pmod software (PMOD TECHNOLOGIES LLC, Zürich, Switzerland). The regions-of-interest (ROI) were calculated to determine the average ^{111}In-DOTA-IA uptake activity in the pHIFU treated VX2 tumors and the control tumors.

2.8 Statistical Analysis

The correlation study between the therapeutic effects of pHIFU and the thermal parameters was performed on 37 treated locations on both hind limbs of six rabbits. Two-sample t-test was used to statistically analyze the correlation of the therapeutic effects of pHIFU and the two thermal parameters, the peak temperature (T_Peak) and the accumulative thermal dose (Dose_CEM43). The positive treatment group consists of 26 locations (N=26) and the negative treatment group consists of 11 locations (N=11). The therapeutic study of enhanced ^{111}In-DOTA-IA delivery in pHIFU treated VX2 tumors was repeated four times in translational rabbit model. The therapeutic results were statistically analyzed in the region of interest by a one-way ANOVA between the pHIFU-treated VX2 tumors (N=4) and the control tumors (N=4). The statistical significance was calculated by the Tukey's method. Data were expressed as mean value and standard deviation, and difference were considered significant at $p < 0.05$.

3. Results

3.1 Correlation between the therapeutic effects of pHIFU treatment and the thermal parameters

To investigate the relation between the therapeutic effect of pHIFU and thermal parameters in bulky normal muscle tissues, we performed total 37 pHIFU treatments on both hind limbs of six female New Zealand white rabbits, with a customized MRI/MR thermometry-guided

preclinical HIFU unit (RK-100). In each experiment, T2-weighted images (Fig. 1a) were acquired before pHIFU procedure to provide the anatomical information of the target area in the hind limb of the rabbit, which provided the necessary guidance for the pHIFU treatment. During pHIFU treatment, the focused spot was placed against the hind limb of the rabbit. Several locations on the hind limb were chosen under the guidance of T2 weighted images to receive the pHIFU treatment (Spot 1–6 on Fig. 1a). During each pHIFU treatment, 120–240 pulses were delivered to the targeted spot at peak acoustic power in the range of 60–90W and duty cycle in the range of 5–20% to induce different pHIFU treatment parameter sets for targeted therapeutic effects. The acoustic parameters and the calculated thermal parameters for each of the six pHIFU treated spots were collectively listed in Table 1. The acoustic intensity around the focused spot and the pHIFU induced temperature change was controlled and monitored in near real-time by using MR-thermometry (Fig. 1b). The temperature change curve and the accumulative thermal dose in the treated location for a typical pHIFU treatment were shown in Fig. 1c. The peak temperature (T_Peak) and the thermal dose (Dose_CEM43) may vary in each animal study and each pHIFU treatment, depending on the location of the target, the acoustic intensity, the duty cycle, number of sonication pulses and the animal response to the pHIFU treatment. For all the spots receiving the pHIFU treatments, the peak temperature T_Peak and the total thermal dose Dose_CEM43 were collectively shown in Fig. 1d, from which the difference of T_Peak and Dose_CEM43 for each spot can be identified. After the pHIFU treatment, another T2-weighted MRI scanning was performed immediately to detect edema created by pHIFU in comparison with the T2-weighted images acquired before pHIFU treatment. Among the six pHIFU treated spots (1–6), three of them present visible edemas (Fig. 1e) in the T2-weigthed images 0 hours after pHIFU treatments. The size and shape of the instantaneous edemas correlate well with the heat distribution (Fig. 1b) during the pHIFU treatments. The peak temperature ranges from 47.01°C to 47.92°C, and the thermal dose ranges from 12.93 to 30.15 for the three spots with visible edemas (Fig. 1d). On the contrast, the peak temperature ranges from 44.2°C to 45.95°C, and the thermal dose ranges from 1.75 to 8.3 for the other three spots without edemas (Fig. 1d) on the T2-weigthed images 0 hours after pHIFU treatments. The instantaneous edema may extend beyond the boundaries of the edemas in the direction of the muscle fiber after pHIFU treatment, which was shown in the followup T2-weighted images acquired 24 hours after pHIFU treatments (Fig. 1f).

T1-weighted contrast enhanced (CE) images were extracted from the DCEMRI series 7 min after bolus injection was used to analyze the improved contrast uptake in the regions of interest. Binary tissue response (True/False) was determined by analyzing the presence of improved contrast uptake in the regions of interest on the T1-weighted CE images 24 hours after pHIFU treatment (Fig. 2a), in comparison with the T1-weighted CE images 0 hours after pHIFU treatment. It was noticed that the three spots demonstrated with edema 0 hours after the pHIFU treatments eventually lead to the improved contrast uptake in the regions of interest, while contrast uptake improvement was absent in the other three spots where no edema showed up in the T2-weigthed MRI images 0 hours after pHIFU treatments. For the same three spots with edema demonstrated at 0 hours after the pHIFU treatments, changes in the permeability k^{trans} were noticed by comparing these tissue parameters fitted from Kety model at 0 hours and 24 hours after pHIFU treatment (Fig 2b).

The peak temperature, the thermal dose and the binary tissue response for each of the total 37 pHIFU treatments were plotted collectively in Fig. 3. As shown in Fig. 3, most pHIFU treatments with higher peak temperature and higher thermal dose presented enhanced contrast uptake while the chance of showing positive response to the pHIFU treatments was low for the cases with low peak temperature and low thermal dose. The therapeutic effects of the total 37 pHIFU treatments and the corresponding thermal parameters were further statistically analyzed by two-sample t-test. The peak temperature (T_Peak) and the accumulative thermal dose (Dose_CEM43) of both positive treatment group and negative treatment group were listed as mean values and standard deviation in the table (Tab. 2). We also investigated thresholds that can reliably identify successful outcomes. This was done by investigating a threshold that maximizes both sensitivity and specificity. Statistical analysis showed that the threshold T_Peak = 46°C yielded 83% sensitivity and 75% specificity based on the data (26 positive pHIFU treatments and 11 negative pHIFU treatments). Similarly, the threshold Dose_CEM43 = 12.6 yielded 86% sensitivity and 88% specificity. The calculated p-values for both T_Peak and Dose_CEM43 were below 0.001, which indicated statistical significance of the results.

3.2 Enhanced delivery of ^{111}In-DOTA-IA in VX2 tumors pretreated by pHIFU

Following the study in bulky normal muscle tissues of rabbit model to validate the correlation between the therapeutic effects of pHIFU treatment and the thermal parameters, we further explored the feasibility to use pHIFU treatments to enhance tumor permeability in bulky VX2 tumors implanted on the hind limb of rabbits. Four female New Zealand white rabbits implanted with VX2 tumors on both sides eventually entered the whole procedure, including pHIFU treatments, systemic ^{111}In-DOTA-IA delivery and SPECT scanning. Before any pHIFU procedure, T2-weighted images (Fig. 4a) were acquired for each rabbit implanted with VX2 tumors to validate the growth and the size of the VX2 tumors on both sides. Same as in the mechanism study based on bulky normal muscle tissue of rabbit model, another set of T2-weighted images (Fig. 4b) was acquired immediately before pHIFU procedure to provide the anatomical information of the target tumor in the hind limb of the rabbit, which were then used jointly with RK100 control software to provide the necessary guidance for the pHIFU treatment. During pHIFU treatment, the focused spot was placed against the targeted VX2 tumor. 4–6 spots with several millimeters in distance were chosen in the VX2 tumors to receive pHIFU treatments, which ensured the coverage of pHIFU treatments on the entire VX2 tumors. The acoustic intensity around the focused spot and the HIFU induced temperature change was controlled and monitored in near real-time by using MR-thermometry (Fig. 4c). The treatment parameters such as acoustic intensity, duty cycles and number of pulses might be tuned a little bit to ensure the target area reach the expected temperature change and receive sufficient thermal dose (Fig. 4d) already optimized in the correlation study with bulky normal muscle tissues.

24 hours after receiving pHIFU treatment, the rabbit was injected with the small molecule $\alpha_v\beta_3$ targeting radiopharmaceutical ^{111}In-DOTA-IA via the vein in the ear. The ^{111}In-DOTA-IA was synthesized in the house by radiolabeling tumor targeting IA with ^{111}In using DOTA as a bifunctional chelator (Supplementary Fig. 1 and Fig. 2). The DOTA-IA was radiolabeled with 111In at >96% radiochemical yield and the radiochemical purity was over

99.5% without any purification. The specific activity of ^{111}In-DOTA-IA was calculated to be in the range of 1050–1200 μCi/μg. Another 24 hours after ^{111}In-DOTA-IA injection, the radiopharmaceutical uptake of the rabbit in the VX2 tumors was imaged by SPECT scanning. The two legs of the rabbit spread out against the bed in prone position to ensure both VX2 tumors can be covered in the SPECT scanning. The MIP images formed from the reconstructed 3-D results showed the obvious improved uptake in the VX2 tumor pre-treated by pHIFU, in comparison with the control VX2 tumor (Fig. 4e). The regions-of-interest (ROI) were further analyzed with pmod software to determine the average ^{111}In-DOTA-IA uptake activity in the pHIFU treated VX2 tumors and the control tumors. The coronal section images cross the center of the VX2 tumor was shown in Fig. 4f, and the ^{111}In-DOTA-IA uptake activity results for the four rabbits in the pHIFU treatment group and the control group were statistically analyzed as the mean value and standard deviation (Fig. 4g). The uptake of ^{111}In-DOTA-IA in the VX2 tumor pre-treated by pHIFU was improved by 34.5%±19.7% on average, in comparison with the control VX2 tumor, which is statistically significant (N=4, p=0.02).

4. Discussions

This study further investigated the relationship between the therapeutic effects of pHIFU treatment and thermal parameters with in a rabbit model and a preclinical HIFU system RK100, which is much less expensive than a comparative clinical unit like ExAblate used before. A study performed previously with a clinical HIFU system has demonstrated poor correlation in statistics between acoustic parameters and therapeutic pHIFU effect, although different acoustic parameters were used in 179 pHIFU treatments on 25 rabbits to confirm mechanical mechanism of pHIFU enhanced tissue permeability[16, 20]. Instead, a correlation between therapeutic effect and thermal parameters has been revealed on rabbit model. This finding differs significantly from the results reported in previous mouse studies and deserves further verification using a different HIFU system.

We and others have demonstrated that $\alpha_v\beta_3$ targeted ^{111}In showed an improved tumor targeting kinetics with rapid accumulation and prolonged retention in the $\alpha_v\beta_3$ receptor-positive tumor.[24] In order to further increase ^{111}In-DOTA-IA tumor targeting, we developed a novel way to non-invasively increase drug delivery to solid tumors using pHIFU.[10, 11, 13, 25] We have demonstrated that we can use pHIFU to gently heat tumors and surrounding normal tissue to non-toxic temperatures at the depth and time of our choosing, resulting in a multiple-fold increased drug delivery in the targeted area. Of translational significance, this approach uses FDA-approved ultrasound devices and can easily be translated into clinical practice. Our study results confirmed the correlation between therapeutic effect and thermal parameters in a large animal model, and the correlation is replicable in a pre-clinical HIFU system. However, T_Peak=46°C and Dose_CEM43 = 12.6 were found in our study to be the thresholds for most likely successful pHIFU treatment, which was statistically chosen by maximizing both sensitivity and specificity. In contrast, T_Peak=49.36°C and Dose_CEM43 = 159 were found in previous study to partition treatments into high chance and low chance of success in contrast uptake improvement in the bulky tissue treated by pHIFU.[16] The cause for the variations of the thresholds of T_Peak and Dose_CEM43 for high chance of successful pHIFU treatments may be due to

the averaged 2.75 ± 1 °C decrease in peripheral temperature from the core temperature in the rabbit during pHIFU treatment. The measured temperature and the calculated thermal dose in our study was based on the core temperature in the rabbit monitored by a rectal probe during pHIFU treatment, while the difference between the baseline peripheral temperature and the core temperature was not taken into consideration in the post-processing of the MR thermometry data. By taking into account the possible 2.75 ± 1 °C difference in the baseline temperature between core and peripheral sites, the re-calculated T_Peak is 48.75°C and Dose_CEM43 is 84.8, which is in good agreement with the previous findings (T_Peak=49.36°C and Dose_CEM43 = 159) considering ± 1 °C measurement error in MR thermometry.

Based on the findings of the correlation study on bulky normal muscle tissues in a rabbit model, the optimized pHIFU treatment parameters were used to treat VX2 tumors. Compared with normal muscle tissues, tumors already have enhanced permeability and inflammation, and the response to the pHIFU treatments is less dramatic. For example, tissue permeability can be improved above 70% in normal muscle tissues, while it can be improved only around 30% in most cases in the VX2 tumors. HIFU technology has already been used to ablate VX2 tumors.[26] Our technique adapted from ablative HIFU technology requires little change in traditional HIFU system and can be rapidly translated into clinic. Also our technique uses only a fraction of HIFU energy used for ablation and should be safer for clinical use. The combination of pHIFU enhanced delivery strategy and different therapeutic agents could improve efficacy of these agents leading to lower effective systemic dose and lowering the chances of adverse effects.

In this study, SPECT images were acquired 24 hours after radiopharmaceutical injection in this study to demonstrate that pHIFU can induce enhanced delivery of ^{111}In-DOTA-IA to the VX2 tumor. However multiple time points' SPECT scan and extensive biodistribution studies of ^{111}In-DOTA-IA after pHIFU treatment and radiopharmaceutical injection can be conducted in the following studies to help optimize our approach to treat VX2 tumor. Furthermore, we have focused on evaluating pHIFU induced permeability change in normal muscle tissue and VX2 tumor tissue using contrast enhanced MRI and SPECT scan, respectively. In the following studies, additional tools including histological analysis can be used to exam the change in tumor vascularity after pHIFU treatment.

In summary, we have demonstrated that we are able to use MRI/MR thermometry to guide and monitor pHIFU treatment for successful pHIFU mediated drug delivery to both bulky normal muscle tissues and VX2 tumors in a rabbit model. With bulky normal muscle tissues, we have validated the correlation between the therapeutic effects of pHIFU treatment and thermal parameters in this study. The subsequent study based on quantitative SPECT imaging of pHIFU mediated ^{111}In-DOTA-IA delivery to VX2 tumors shows the uptake of ^{111}In-DOTA-IA in the VX2 tumor pre-treated by pHIFU can be improved by 34.5%±19.7% on average, in comparison with the control VX2 tumor. The findings in this study should encourage further efforts in translating this promising technology into clinical use.

Supplementary Material

Refer to Web version on PubMed Central for supplementary material.

Acknowledgments

This work was supported by a grant of the National Institute of Biomedical Imaging and Bioengineering (NIBIB) (R01 EB009009). We thank Ms. Debra Fuller and Sandra Kaminsky for their technical support in MRI scan. We thank Mr. John Richardson for his technical support in SPECT scan. We thank Ms. Dongqin Zhu and Stephanie Rideout for their support in the animal work.

Appendix

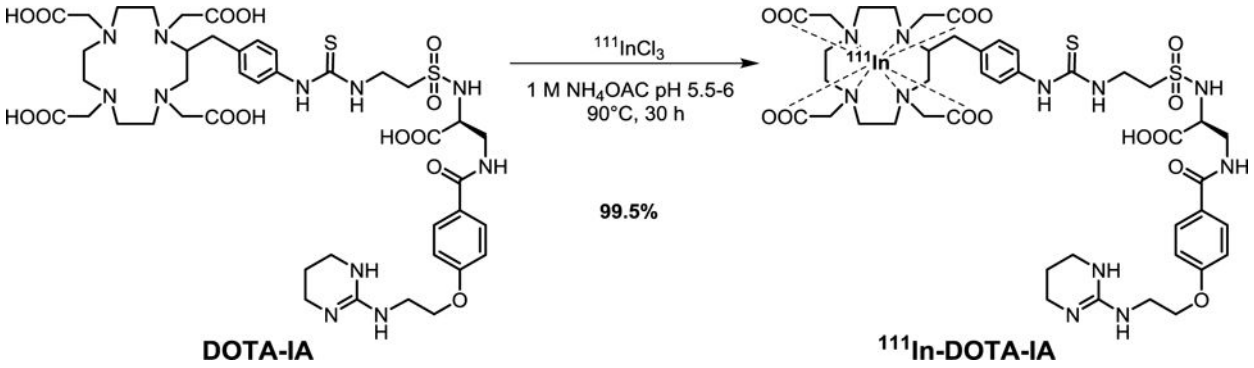

Fig. 1.
Radiochemical synthesis of ^{111}In-DOTA-IA.[22, 23]

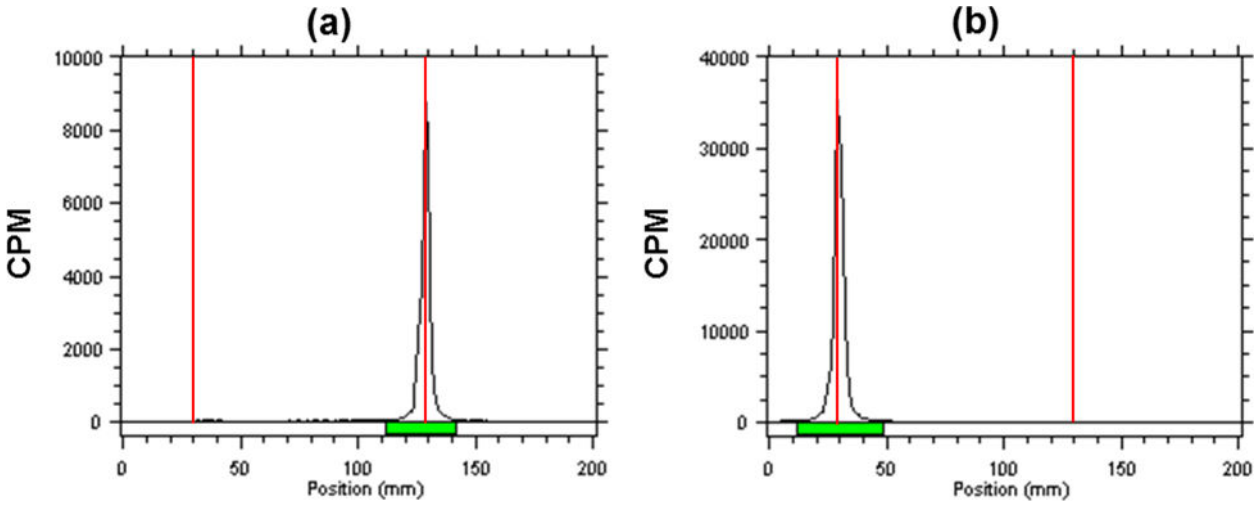

Fig. 2.
Quality control of ^{111}In-DOTA-IA. Un-chelated ^{111}In eluted with the solvent front (Rf = 1) (a); the ^{111}In-DOTA-IA remained at the origin (Rf = 0)

References

1. Kennedy JE. High-intensity focused ultrasound in the treatment of solid tumours. Nature Reviews Cancer. 2005; 5:321–327. [PubMed: 15776004]

2. Vaezy S, Fujimoto VY, Walker C, Martin RW, Chi EY, Crum LA. Treatment of uterine fibroid tumors in a nude mouse model using high-intensity focused ultrasound. American journal of obstetrics and gynecology. 2000; 183:6–11. [PubMed: 10920300]

3. Stewart EA, Rabinovici J, Tempany C, Inbar Y, Regan L, Gastout B, Hesley G, Kim HS, Hengst S. Clinical outcomes of focused ultrasound surgery for the treatment of uterine fibroids. Fertility and sterility. 2006; 85:22–29. [PubMed: 16412721]

4. Wu F, Wang ZB, Cao YD, Chen W, Bai J, Zou J, Zhu H. A randomised clinical trial of high-intensity focused ultrasound ablation for the treatment of patients with localised breast cancer. British journal of cancer. 2003; 89:2227–2233. [PubMed: 14676799]

5. Kennedy J, Wu F, Ter Haar G, Gleeson F, Phillips R, Middleton M, Cranston D. High-intensity focused ultrasound for the treatment of liver tumours. Ultrasonics. 2004; 42:931–935. [PubMed: 15047409]

6. Illing R, Kennedy J, Wu F, Ter Haar G, Protheroe A, Friend P, Gleeson F, Cranston D, Phillips R, Middleton M. The safety and feasibility of extracorporeal high-intensity focused ultrasound (hifu) for the treatment of liver and kidney tumours in a western population. British journal of cancer. 2005; 93:890–895. [PubMed: 16189519]

7. Thüroff S, Chaussy C, Vallancien G, Wieland W, Kiel HJ, le Duc A, Desgrandchamps F, de la Rosette JJ, Gelet A. High-intensity focused ultrasound and localized prostate cancer: Efficacy results from the european multicentric study. Journal of endourology. 2003; 17:673–677. [PubMed: 14622488]

8. Blana A, Walter B, Rogenhofer S, Wieland WF. High-intensity focused ultrasound for the treatment of localized prostate cancer: 5-year experience. Urology. 2004; 63:297–300. [PubMed: 14972475]

9. Yuh EL, Shulman SG, Mehta SA, Xie J, Chen L, Frenkel V, Bednarski MD, Li KCP. Delivery of systemic chemotherapeutic agent to tumors by using focused ultrasound: Study in a murine model1. Radiology. 2005; 234:431–437. [PubMed: 15671000]

10. Dittmar KM, Xie J, Hunter F, Trimble C, Bur M, Frenkel V, Li KCP. Pulsed high-intensity focused ultrasound enhances systemic administration of naked DNA in squamous cell carcinoma model: Initial experience1. Radiology. 2005; 235:541–546. [PubMed: 15798154]

11. Frenkel V, Etherington A, Greene M, Quijano J, Xie J, Hunter F, Dromi S, Li KCP. Delivery of liposomal doxorubicin (doxil) in a breast cancer tumor model: Investigation of potential enhancement by pulsed-high intensity focused ultrasound exposure. Academic radiology. 2006; 13:469–479. [PubMed: 16554227]

12. Khaibullina A, Jang BS, Sun H, Le N, Yu S, Frenkel V, Carrasquillo JA, Pastan I, Li KCP, Paik CH. Pulsed high-intensity focused ultrasound enhances uptake of radiolabeled monoclonal antibody to human epidermoid tumor in nude mice. Journal of Nuclear Medicine. 2008; 49:295–302. [PubMed: 18199622]

13. Frenkel V, Oberoi J, Stone MJ, Park M, Deng C, Wood BJ, Neeman Z, Horne MD III, Li KCP. Pulsed high-intensity focused ultrasound enhances thrombolysis in an in vitro model1. Radiology. 2006; 239:86–93. [PubMed: 16493016]

14. Stone MJ, Frenkel V, Dromi S, Thomas P, Lewis RP, Li KCP, Horne MD, Wood BJ. Pulsed-high intensity focused ultrasound enhanced tpa mediated thrombolysis in a novel< i> in vivo</i> clot model, a pilot study. Thrombosis research. 2007; 121:193–202. [PubMed: 17481699]

15. Sheikov N, McDannold N, Vykhodtseva N, Jolesz F, Hynynen K. Cellular mechanisms of the blood-brain barrier opening induced by ultrasound in presence of microbubbles. Ultrasound Med Biol. 2004; 30:979–989. [PubMed: 15313330]

16. O'Neill BE, Vo HQ, Shao H, Karmonik C, Zhou X, Li KC. Mri-based prediction of pulsed high-intensity focused ultrasound effect on tissue transport in rabbit muscle. Journal of Magnetic Resonance Imaging. 2013; 38:1094–1102. [PubMed: 23553784]

17. Watson KD, Lai CY, Qin S, Kruse DE, Lin YC, Seo JW, Cardiff RD, Mahakian LM, Beegle J, Ingham ES, Curry FR, Reed RK, Ferrara KW. Ultrasound increases nanoparticle delivery by reducing intratumoral pressure and increasing transport in epithelial and epithelial-mesenchymal transition tumors. Cancer Res. 2012; 72:1485–1493. [PubMed: 22282664]

18. O'Neill BE, Vo H, Angstadt M, Li KPC, Quinn T, Frenkel V. Pulsed high intensity focused ultrasound mediated nanoparticle delivery: Mechanisms and efficacy in murine muscle. Ultrasound in Medicine & Biology. 2009; 35:416–424. [PubMed: 19081668]

19. O'Reilly MA, Waspe AC, Chopra R, Hynynen K. Mri-guided disruption of the blood-brain barrier using transcranial focused ultrasound in a rat model. JoVE (Journal of Visualized Experiments). 2012:e3555–e3555.

20. O'Neill BE, Karmonik C, Sassaroli E, Li KC. Estimation of thermal dose from mr thermometry during application of nonablative pulsed high intensity focused ultrasound. Journal of Magnetic Resonance Imaging. 2012; 35:1169–1178. [PubMed: 22170785]

21. Sapareto SA, Dewey WC. Thermal dose determination in cancer therapy. Int J Radiat Oncol Biol Phys. 1984; 10:787–800. [PubMed: 6547421]

22. Jang BS, Lim E, Hee Park S, Shin IS, Danthi SN, Hwang IS, Le N, Yu S, Xie J, Li KC, Carrasquillo JA, Paik CH. Radiolabeled high affinity peptidomimetic antagonist selectively targets alpha(v)beta(3) receptor-positive tumor in mice. Nucl Med Biol. 2007; 34:363–370. [PubMed: 17499725]

23. Burnett CA, Xie J, Quijano J, Shen Z, Hunter F, Bur M, Li KC, Danthi SN. Synthesis, in vitro, and in vivo characterization of an integrin alpha(v)beta(3)-targeted molecular probe for optical imaging of tumor. Bioorg Med Chem. 2005; 13:3763–3771. [PubMed: 15863003]

24. Lijowski M, Caruthers S, Hu G, Zhang H, Scott MJ, Williams T, Erpelding T, Schmieder AH, Kiefer G, Gulyas G, Athey PS, Gaffney PJ, Wickline SA, Lanza GM. High sensitivity: High-resolution spect-ct/mr molecular imaging of angiogenesis in the vx2 model. Invest Radiol. 2009; 44:15–22. [PubMed: 18836386]

25. Bednarski MD, Lee JW, Callstrom MR, Li KC. In vivo target-specific delivery of macromolecular agents with mr-guided focused ultrasound. Radiology. 1997; 204:263–268. [PubMed: 9205257]

26. Kim KW, Lee JY, Lee JM, Jeon YS, Choi YS, Park J, Kim H, Han JK, Choi BI. High-intensity focused ultrasound ablation of soft-tissue tumors and assessment of treatment response with multiparametric magnetic resonance imaging: Preliminary study using rabbit vx2 tumor model. Journal of Medical Ultrasound. 2014; 22:99–105.

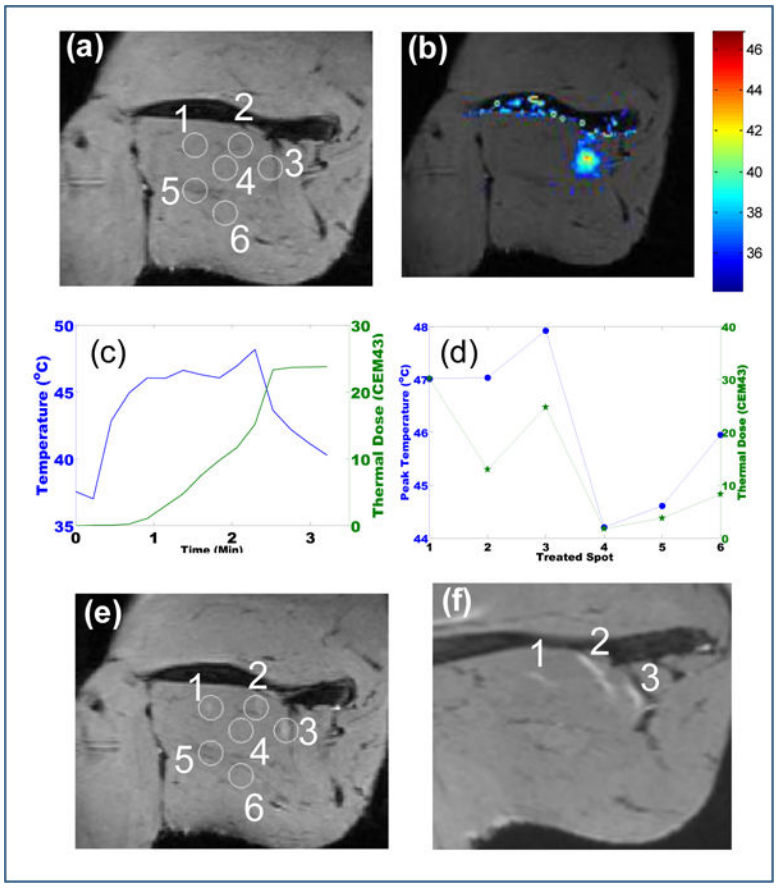

Fig. 1.

pHIFU treatment resulting in enhanced Magnevist uptake in the thigh muscle of normal rabbit. Total six spots (1–6) are treated. **(a)** The coronal T2 image in the treatment plane prior to the pHIFU treatment; **(b)** MR thermometry map during the pHIFU treatment; **(c)** The local temperature change (Blue) and accumulative thermal dose (Green) along with the pHIFU treatment; **(d)** The peak temperature (Blue) and the total thermal dose (Green) for the six spots under pHIFU treatment; **(e)** The corresponding coronal T2 image in the treatment plane immediately after the pHIFU treatment. Edema occurred in 3 treated spots; **(f)** The corresponding was absent in the other three spots coronal T2 image in the treatment plane 24 hours after the pHIFU treatment. The edema of the three successfully treated spots (1–3) spread along the muscle fiber.

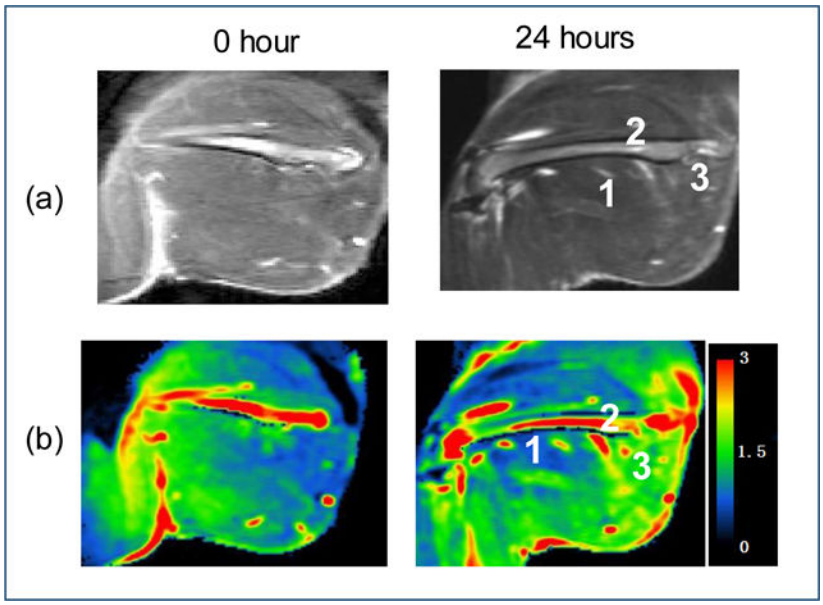

Fig. 2.

Permeability change in the thigh muscle of normal rabbit treated by pHIFU. **(a)** The T1 image in the treatment plane 0 hours (left) and 24 hours (right) after the pHIFU treatment; **(b)** Ktrans map in the treatment plane 0 hours (left) and 24 hours (right) after the pHIFU treatment;

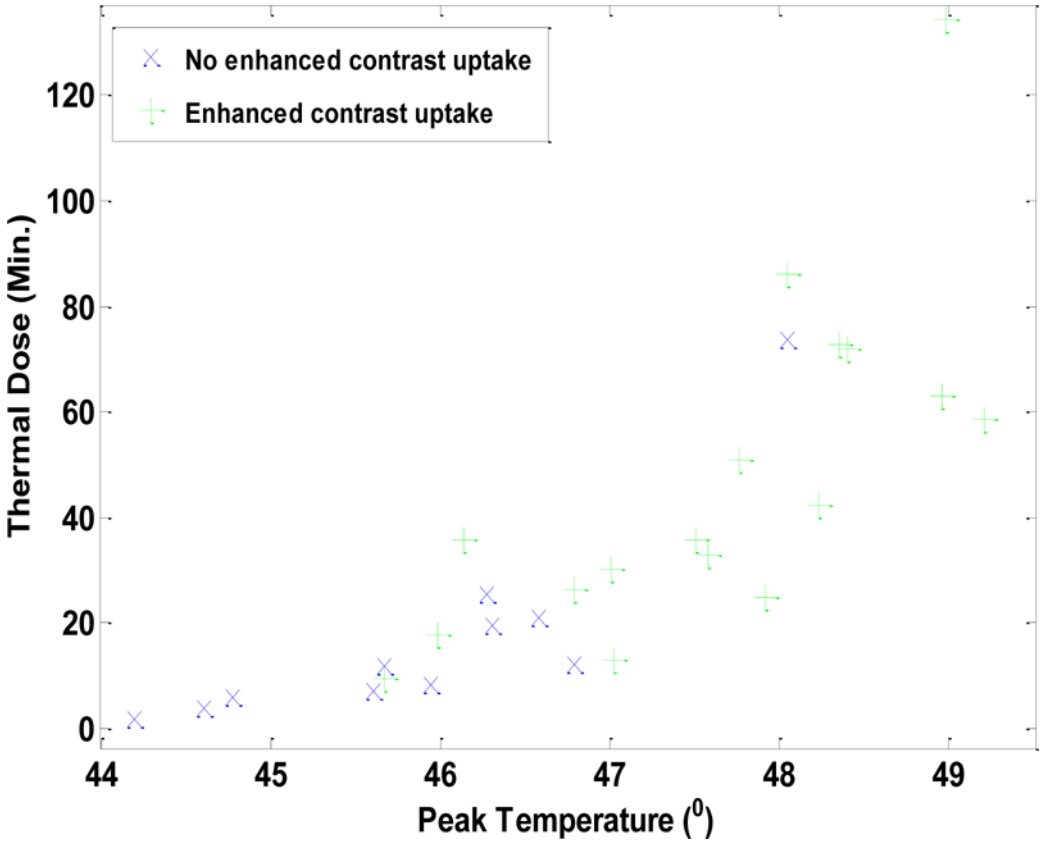

Fig. 3.

Distribution of pHIFU assisted drug delivery on normal rabbit muscle with different peak temperature and the thermal dose

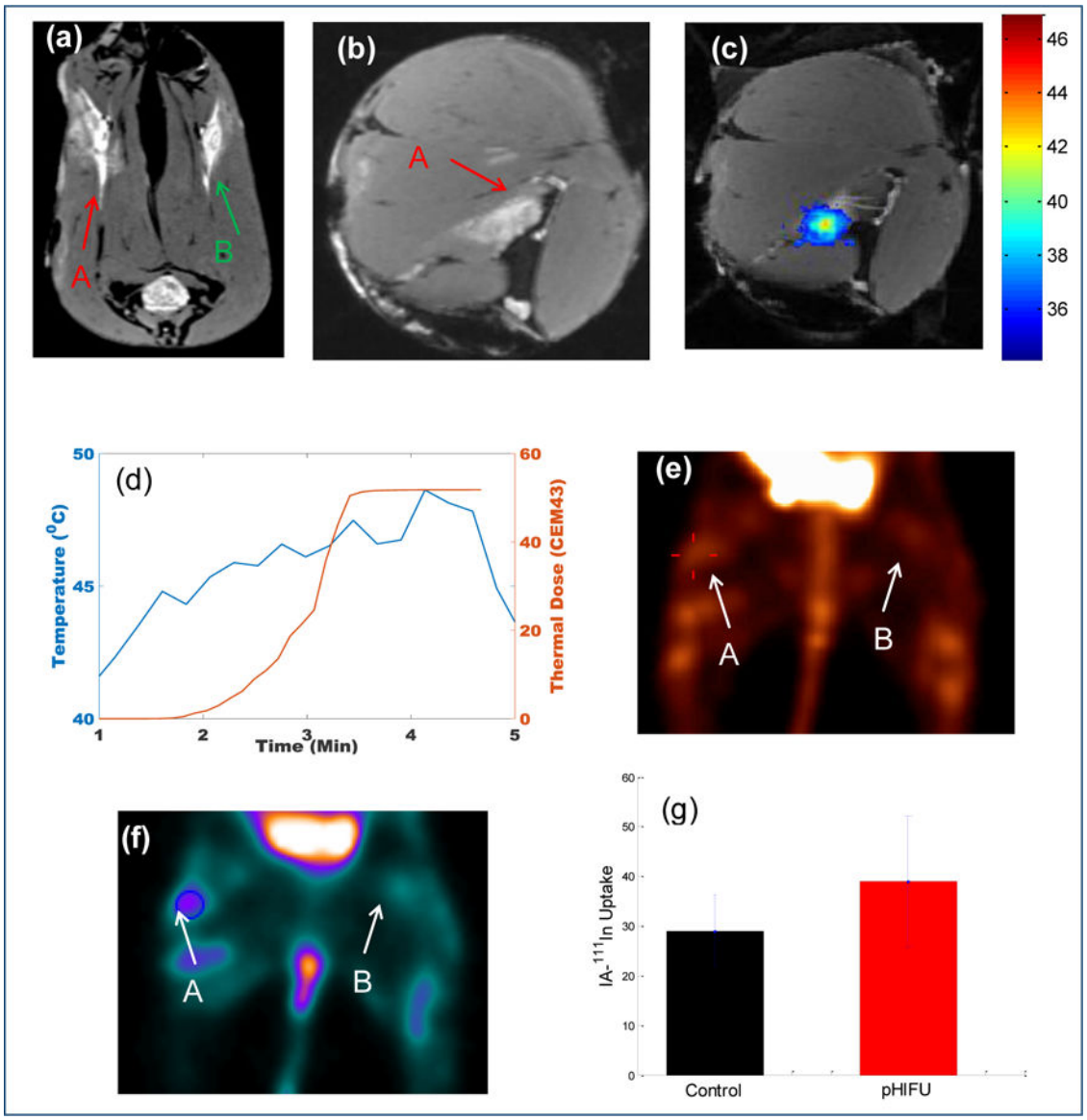

Fig. 4.

MRI/MR thermometry guided pHIFU treatment of VX2 tumor in the rabbit thigh. A and B is the target tumor on the right side for pHIFU treatment and the control tumor on the left side, respectively. **(a)** Cross-section MRI images of the VX2 tumors on both rabbit thighs, **(b)** Coronal-section MRI image of the target VX2 tumor on the right thigh; **(c)** MR thermometry map during the pHIFU treatment; **(d)** The local temperature change and the thermal dose along with the pHIFU treatment; **(e)** MIP images of the SPECT scan 24hrs after the injection of ^{111}In-DOTA-IA; **(f)** Coronal image of the SPECT scan in the plane of VX2 tumors 24hrs after the injection of ^{111}In-DOTA-IA. **(g)** Statistical analysis of the uptake of ^{111}In-DOTA-IA in the region of interest treated by pHIFU as compared to the untreated tumor spot (n=4, p=0.02).

Table 1

The acoustic parameters and calculated thermal parameters from MR thermometry data of the six spots in the thigh muscle of normal rabbit being treated by pHIFU. P^{Av} is calculated by $P^{Av} = P^{Peak} \times DC$, and E^{total} is calculated by $E^{total} = P^{Av} \times Pulses$.

No.	P^{Peak}	DC	Pulses	P^{Av}	E^{total}(J)	T_Peak	Dose_CEM43
1	67.5	20%	240	13.5	3240	47.01	30.15
2	90	10%	120	9	1080	47.03	12.93
3	90	5%	120	4.5	540	47.92	24.73
4	60	5%	120	3	360	44.2	1.75
5	60	5%	220	3	660	44.61	3.76
6	90	5%	120	4.5	540	45.95	8.30

J Control Release. Author manuscript; available in PMC 2018 July 16.

Table 2

The mean and standard deviation (SD) of the variables of interest in each group. The p-values are based on a two-sample t-test for T_Peak and $\log_{10}$(Dose_CEM43), and based on a Mann-Whitney test for Dose_CEM43. The threshold was statistically chosen by maximizing both sensitivity and specificity. It was found that the threshold T_Peak = 46 yielded 83% sensitivity and 75% specificity based on our data. Similarly, the threshold Dose_CEM43 = 12.6 yielded 86% sensitivity and 88% specificity.

	Negative (N=11)		Positive (N=26)		
Variable	**Mean**	**SD**	**Mean**	**SD**	**P-value**
T_Peak	45.9	1.1	48.6	1.9	<0.001
Dose_CEM43	17.3	20.1	159.3	363.7	<0.001
$\log_{10}$(Dose_CEM43)	1.038	0.440	1.831	0.499	<0.001